IOPscience iopscience.iop.org

Home Search Collections Journals About Contact us My IOPscience

Effects of interactions in two dimensions

This article has been downloaded from IOPscience. Please scroll down to see the full text article.

2009 J. Phys. A: Math. Theor. 42 214010

(http://iopscience.iop.org/1751-8121/42/21/214010)

View the table of contents for this issue, or go to the journal homepage for more

Download details:
IP Address: 171.66.16.154
The article was downloaded on 03/06/2010 at 07:48

Please note that terms and conditions apply.

J. Phys. A: Math. Theor. **42** (2009) 214010 (10pp) doi:10.1088/1751-8113/42/21/214010

Effects of interactions in two dimensions

A A Shashkin[1], A A Kapustin[1], E V Deviatov[1], V T Dolgopolov[1], Z D Kvon[2] and S V Kravchenko[3]

[1] Institute of Solid State Physics, Chernogolovka, Moscow District 142432, Russia
[2] Institute of Semiconductor Physics, Novosibirsk 630090, Russia
[3] Physics Department, Northeastern University, Boston, Massachusetts 02115, USA

E-mail: s.kravchenko@neu.edu

Received 15 October 2008
Published 8 May 2009
Online at stacks.iop.org/JPhysA/42/214010

Abstract
Strong electron–electron interactions in dilute two-dimensional electron systems in silicon lead to Pauli spin susceptibility growing critically at low electron densities. This effect originates from renormalization of the effective mass rather than the g-factor. The relative mass enhancement is system and disorder independent, which suggests that it is determined by electron–electron interactions only.

PACS numbers: 71.30.+h, 73.40.Qv, 71.18.+y

(Some figures in this article are in colour only in the electronic version)

1. Introduction

Low-temperature transport in many clean two-dimensional (2D) electron systems manifests critical behavior known as 2D metal–insulator transition [1–3]. This phenomenon takes place at low carrier densities, where the ratio of the Coulomb and Fermi energies $r_s = E_C/E_F \gg 1$, and therefore, interactions play a crucial role. The 2D electron system in silicon turns out to be a very convenient object for studies of the strongly correlated regime due to the large interaction strengths (at electron densities $n_s \sim 10^{11}$ cm^{-2}, the interaction parameter reaches $r_s \sim 15$) and high homogeneity of the samples. (To reach the same interaction strengths in n-type GaAs/AlGaAs heterostructures, one would need to work at electron densities $n_s < 10^9$ cm^{-2}—such samples are not readily available as of yet.) Silicon has the additional advantage that its electron spectrum has two almost degenerate valleys, which further enhances the correlation effects. In (1 0 0) silicon MOSFETs, spin susceptibility of band electrons (Pauli spin susceptibility) becomes enhanced by almost an order of magnitude at low electron densities, growing critically near a sample-independent density $n_\chi \approx 8 \times 10^{10}$ cm^{-2}. Such behavior is characteristic in the close vicinity of a phase transition. Interestingly, this dramatic increase of the spin susceptibility is due to the strong renormalization of the effective mass

1751-8113/09/214010+10$30.00
© 2009 IOP Publishing Ltd Printed in the UK

while the g-factor remains practically constant and close to its band value. The effective mass has also been measured in a dilute two-dimensional electron system in (1 1 1) silicon. The mass renormalization as a function of the interaction parameter r_s is in good agreement with that measured in (1 0 0) silicon, indicating that the relative mass enhancement is system and disorder independent, and is determined by electron–electron interactions only.

2. Experimental setup and samples

Measurements were made in an Oxford dilution refrigerator on two groups of samples. Low-disordered (1 0 0) silicon metal-oxide-semiconductor field-effect transistors (MOSFETs) were provided by T M Klapwijk (Kavli Institute of Nanoscience, TU Delft). The silicon oxide layer was grown repeatedly during several stages of fabrication to decrease the number of charged impurities and obtain a high-quality interface; as a result, in samples with an oxide thickness of 149 nm, peak mobilities of 3 $m^2 V^{-1} s^{-1}$ were achieved at $T = 100$ mK. The second advantage of these samples is a very low contact resistance (in 'conventional' silicon samples, high contact resistance becomes the main experimental obstacle in the low-density/low-temperature limit). To minimize the contact resistance, thin slits in the gate metalization have been introduced, which allows for maintaining high electron density near the contacts regardless of its value in the main part of the sample. The second group of samples consisted of more disordered (1 1 1) silicon MOSFETs similar to those previously used in [4]. Oxide thickness in these samples was equal to 154 nm. In highest-mobility samples, the normal of the sample surface was tilted from the [1 1 1] toward the [1 1 0] direction by a small angle of 8°. Anisotropy for electron transport in such samples does not exceed 5% at $n_s = 3 \times 10^{11}$ cm^{-2} and increases weakly with electron density, staying below 25% at $n_s = 3 \times 10^{12}$ cm^{-2}, as has been determined in independent experiments.

The resistivity ρ was measured by a standard low-frequency lock-in technique. For magnetization measurements, a novel method [5, 6] was used that entails modulating the magnetic field with an auxiliary coil and measuring the ac current induced between the gate and the 2D electron system. The magnetic field B was modulated with a small ac field, δB, in the range 0.005–0.03 T at frequencies between $f = 0.05$ and 0.45 Hz. The in-phase and out-of-phase components of the current between the gate and the 2D electron system were measured with high precision ($\sim 10^{-16}$ A) using a home-made current–voltage converter and a lock-in amplifier. The real (in-phase) component of the current depends on the dissipative conductivity σ of the sample. The imaginary (out-of-phase) current component, under the condition that $2\pi f C \ll \sigma$, is equal to

$$\mathrm{Im}\, i = \frac{2\pi f C}{e} \frac{\mathrm{d}\mu}{\mathrm{d}B} \delta B, \tag{1}$$

where C is the capacitance of the sample measured in the same experiment, and μ is the chemical potential. Use of ultra-low frequencies ensures that $2\pi f C \ll \sigma$, and the out-of-phase current component is not contaminated by lateral transport effects. By applying the Maxwell relation $\mathrm{d}M/\mathrm{d}n_s = -\mathrm{d}\mu/\mathrm{d}B$, one can then obtain the magnetization M from the measured i.

3. Results and discussion

3.1. Spin susceptibility in (1 0 0) silicon

A typical experimental trace of $i(n_s)$ in a parallel magnetic field of 5 T is displayed in figure 1. The inset shows magnetization $M(n_s)$ in the metallic phase obtained by integrating

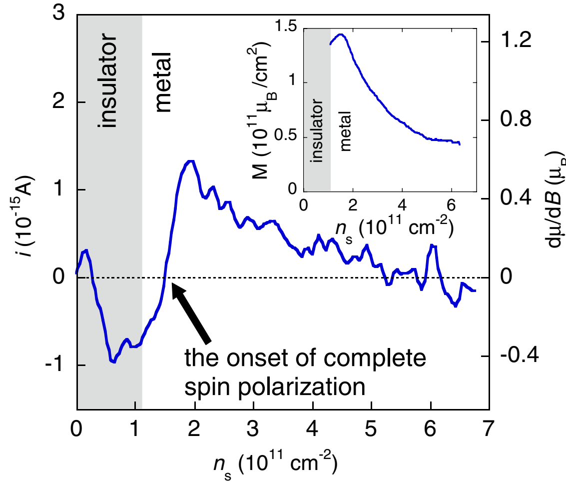

Figure 1. Imaginary current component in the magnetization experiment as a function of the electron density in a magnetic field of 5 T and $T = 0.4$ K. The grey area depicts the insulating phase. Magnetization versus n_s is displayed in the inset. Note that the maximum M is coincident within the experimental uncertainty with $\mu_B n_s$. (From [6].)

$\mathrm{d}M/\mathrm{d}n_s = -\mathrm{d}\mu/\mathrm{d}B$ with the integration constant $M(\infty) = B\chi_0$, where χ_0 is the Pauli spin susceptibility of non-interacting electrons. A nearly anti-symmetric jump of $i(n_s)$ about zero on the y-axis (marked by the black arrow) separates the high- and low-density regions in which the signal is positive and negative ($M(n_s)$ is decreasing and increasing), respectively. Such a behavior is expected based on simple considerations. At low densities, all electrons are spin polarized in a magnetic field, so for the simple case of non-interacting 2D electrons one expects $\mathrm{d}\mu/\mathrm{d}B = -\mu_B$ (at $n_s \to 0$, deep in the insulating regime, the capacitance of the system vanishes and, therefore, the measured current approaches zero). At higher densities, when the electrons start to fill the upper spin subband, $M(n_s)$ starts to decrease, and $\mathrm{d}\mu/\mathrm{d}B$ is determined by the renormalized Pauli spin susceptibility χ and is expected to decrease with n_s due to reduction in the strength of electron–electron interactions. Finally, in the high-density limit, the spin susceptibility approaches its 'non-interacting' value χ_0, and $\mathrm{d}\mu/\mathrm{d}B$ should approach zero. The onset of complete spin polarization—the electron density n_p at which the electrons start to fill the upper spin subband—is given by the condition $\mathrm{d}\mu/\mathrm{d}B = 0$ ($M(n_s)$ reaches a maximum), as indicated by the black arrow in the figure. It is important that over the range of magnetic fields used in the experiment (1.5–7 T), the maximum M coincides within the experimental uncertainty with $\mu_B n_s$, thus confirming that all the electrons are indeed spin polarized below n_p. Note however that the absolute value of $\mathrm{d}\mu/\mathrm{d}B$ at $n_s < n_c$ is reduced in the experiment. This can be attributed to smearing of the minimum in $i(n_s)$ caused by the possible influence of the residual disorder in the electron system, which is crucial in and just above the insulating phase (see below). Another reason for the reduction in $\mathrm{d}\mu/\mathrm{d}B$ is the electron–electron interactions (due to, e.g., the enhanced effective mass).

In figure 2(a), a set of curves is shown for the experimental $\mathrm{d}\mu/\mathrm{d}B$ versus electron density in different magnetic fields. Experimental results in the range of magnetic fields studied do not depend, within the experimental noise, on temperature below 0.6 K (down to 0.15 K which was the lowest temperature achieved in this experiment). The onset of full spin polarization shifts to higher electron densities with an increasing magnetic field. The grey area depicts the insulating phase, which expands somewhat with B. Note that the range of magnetic fields

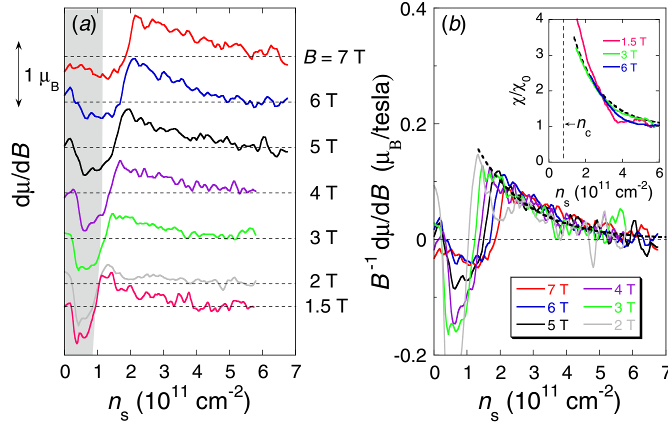

Figure 2. (*a*) The experimental $d\mu/dB$ as a function of electron density in different magnetic fields and $T = 0.4$ K. The curves are vertically shifted for clarity. The grey area depicts the insulating phase. Note that the onset of full spin polarization in our experiment always takes place in the metallic regime. (*b*) Scaling of the $d\mu/dB$ curves, normalized by magnetic field magnitude, at high electron densities. The dashed line represents the 'master curve'. The spin susceptibility obtained by integrating the master curve (the dashed line) and raw data at $B = 1.5$, 3 and 6 T is displayed in the inset. (From [6].)

used in the experiment is restricted from below by the condition that $d\mu/dB$ crosses zero in the metallic regime. In figure 2(*b*), it is shown how these curves, normalized by the magnetic field, collapse in the partially polarized regime onto a single 'master curve'. The existence of such scaling verifies proportionality of the magnetization to B and establishes a common zero level for the experimental traces. Integration of the master curve over n_s yields the spin susceptibility $\chi = M/B$, as shown in the inset to figure 2(*b*). Also shown is the spin susceptibility obtained by integration of raw curves at $B = 1.5$, 3 and 6 T, which, within the experimental error, yield the same dependence.

This method of measuring the spin susceptibility, being the most direct, suffers, however, from the possible influence of the unknown diamagnetic contribution to the measured $d\mu/dB$, which arises from the finite width of the 2D electron layer. To verify that this influence is negligible, another two independent methods to determine χ have been employed. The second method is based on marking the electron density n_p at which $d\mu/dB = 0$ and which corresponds to the onset of complete spin polarization, as mentioned above. The so-determined polarization density $n_p(B)$ can be easily converted into $\chi(n_s)$ via $\chi = \mu_B n_p/B$. Note that in contrast to the value of $d\mu/dB$, the polarization density n_p is practically not affected by the possible influence of the diamagnetic shift. The third method for measuring n_p and χ, insensitive to the diamagnetic shift, relies on analyzing the magnetocapacitance, C. In a high magnetic field, a step-like feature emerges on the $C(n_s)$ curves and shifts to higher electron densities with the increasing field (for the raw experimental data, see [6]). This feature corresponds to the thermodynamic density of states abruptly changing when the electrons' spins become completely polarized. As above, it allows one to determine the electron density of the full spin polarization.

In figure 3, the summary of the results is shown for the Pauli spin susceptibility as a function of n_s, obtained using all three methods described above. The excellent agreement between the results obtained by all of the methods establishes that a possible influence of the diamagnetic shift is negligible and, therefore, the validity of the data including those at the

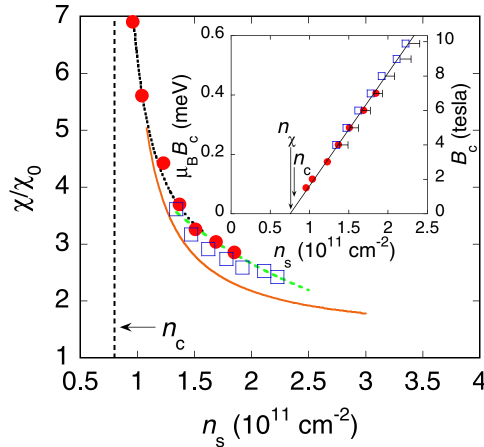

Figure 3. Dependence of the Pauli spin susceptibility on electron density obtained by all three methods described in the text: integral of the master curve (the dashed line), $d\mu/dB = 0$ (circles) and magnetocapacitance (squares). The dotted line is a guide to the eye. Also shown by a solid line is the transport data of [7]. Inset: the polarization field as a function of the electron density determined from the magnetization (circles) and magnetocapacitance (squares) data. The symbol size for the magnetization data reflects the experimental uncertainty, and the error bars for the magnetocapacitance data extend to the middle of the jump in C. The data for B_c are described by a linear fit which extrapolates to a density n_χ close to the critical density n_c for the $B = 0$ MIT. (From [6].)

lowest electron densities is justified. There is also good agreement between these results and the data obtained by the transport experiments of [7]. This adds credibility to the transport data and confirms that full spin polarization occurs at the field B_c; however, it should be noted that evidence for the phase transition can only be obtained from thermodynamic measurements. The magnetization data extend to lower densities than the transport data, and larger values of χ are reached, exceeding the 'non-interacting' value χ_0 by almost an order of magnitude. The Pauli spin susceptibility behaves critically close to n_χ: $\chi \propto n_s/(n_s - n_\chi)$. This is in favor of the occurrence of a spontaneous spin polarization (either Wigner crystal or ferromagnetic liquid) at low n_s, although in currently available samples, the growing disorder at $n_s \sim n_c$ conceals the origin of the low-density phase. In other words, so far, one can only reach an incipient transition to a new phase.

The dependence $B_c(n_s)$, determined from the magnetization and magnetocapacitance data, is represented in the inset to figure 3. The two data sets coincide and are described well by a common linear fit which extrapolates to a density n_χ close to (but slightly below) n_c. In the low-field limit ($B < 1.5$ T), the jump in $d\mu/dB$ shifts to the insulating regime, which does not allow one to approach closer vicinity of n_χ: based on the data obtained in the regime of strong localization, one would not be able to make conclusions concerning properties of a clean metallic electron system.

3.2. The effective mass in (1 0 0) silicon

The effective mass was measured by several methods. The first method was based on the comparison of our data for zero-field resistivity with the theory [8]. It allows us to extract the values of m and g separately [9]. In the second method, we have determined the effective mass by analyzing temperature dependence of the weak-field Shubnikov–de Haas (SdH) oscillations

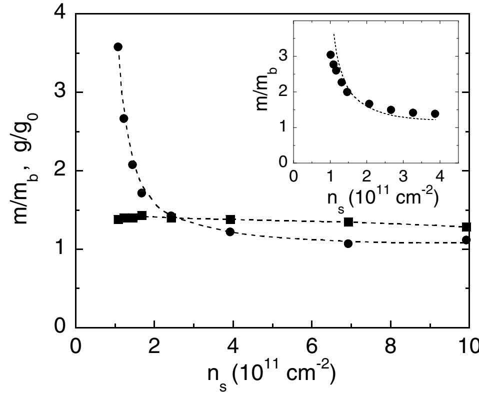

Figure 4. The effective mass (circles) and g-factor (squares), determined from the analysis of the parallel field magnetoresistance and temperature-dependent conductivity, versus electron density. The dashed lines are guides to the eye. The inset compares the so-obtained effective mass (the dotted line) with that extracted from the analysis of SdH oscillations (circles). (From [9, 10].)

[10] (for details of the procedure, see the following subsection). The third method was based on measurements of the magnetization in tilted magnetic fields described in detail in [11]. All three methods gave quantitatively similar results.

In figure 4, we show the values g/g_0 and m/m_b as a function of the electron density (here $g_0 = 2$ is the g-factor in bulk silicon, m_b is the band mass equal to $0.19m_e$, and m_e is the free electron mass). In the high n_s region (relatively weak interactions), the enhancement of both g and m is relatively small, both values slightly increasing with decreasing electron density in agreement with earlier data [12]. Also, the renormalization of the g-factor is dominant compared to that of the effective mass, which is consistent with theoretical studies [13].

In contrast, the renormalization at low n_s (near the critical region), where $r_s \gg 1$, is much more striking. As the electron density is decreased, the renormalization of the effective mass overshoots abruptly while that of the g-factor remains relatively small, $g \approx g_0$, without tending to increase. Hence, the current analysis indicates that it is the effective mass, rather than the g-factor, that is responsible for the drastically enhanced gm value near the metal–insulator transition.

3.3. The effective mass in (1 1 1) silicon

The effective mass in (1 1 1) silicon MOSFETs was determined from the analysis of the Shubnikov–de Haas oscillations. In figure 5(a), we show the magnetoresistance $R_{xx}(B)$ for $n_s = 8.4 \times 10^{11}$ cm^{-2} at different temperatures. In weak magnetic fields, the SdH oscillation period corresponds to a change of the filling factor $\nu = n_s hc/eB$ by $\Delta\nu = 4$, which indicates that both the spin and valley degeneracies are equal to $g_s = g_v = 2$. The fact that the valley degeneracy is equal to $g_v = 2$, rather than $g_v = 6$, is a long-standing problem which lacks a definite answer so far [4].

In figure 5(b), we plot positions of the resistance minima in the (B, n_s) plane. The symbols are the experimental data and the lines are the expected positions of the cyclotron and spin minima calculated according to the formula $n_s = \nu eB/hc$. The resistance minima are seen at $\nu = 6$, 10, 14, 18, 22, 26 and 30 corresponding to spin splittings and at $\nu = 4$, 8, 12, 16, 20, 24 and 28 corresponding to cyclotron gaps. The valley splitting is not seen at low electron densities/weak magnetic fields, and the even numbers of the SdH oscillation

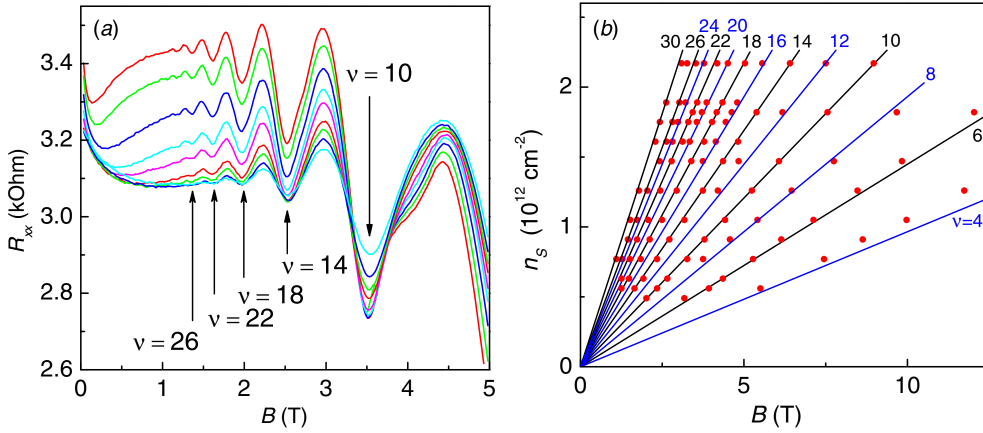

Figure 5. (*a*) Shubnikov–de Haas oscillations in the (1 1 1) Si MOSFET at $n_s = 8.4 \times 10^{11}$ cm^{-2} for the following temperatures (from top to bottom): 0.03, 0.12, 0.2, 0.3, 0.38, 0.47, 0.55, 0.62 and 0.75 K. (*b*) Positions of the SdH oscillation minima in the (B, n_s) plane (dots) and the expected positions of the cyclotron and spin minima calculated according to the formula $n_s = \nu eB/hc$ (solid lines). (From [14].)

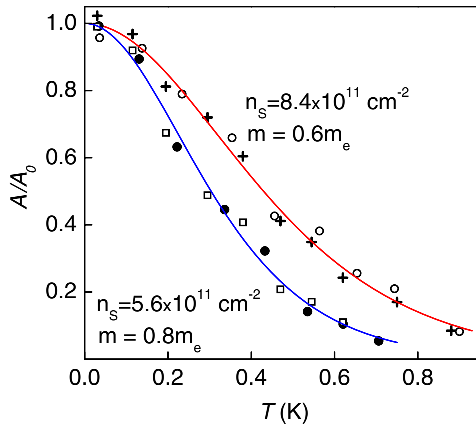

Figure 6. Change of the amplitude of the weak-field SdH oscillations with temperature at different electron densities for magnetic fields $B_1 = 1.44$ T (dots), $B_2 = 1.64$ T (squares) and $B_1 = 1.45$ T (open circles), $B_2 = 1.74$ T (crosses). The value of T for the B_1 data is multiplied by the ratio B_2/B_1. The solid lines are fits using equation (2). (From [14].)

minima confirm the valley degeneracy equal to $g_v = 2$. The spin minima extend to appreciably lower electron densities than the cyclotron minima, behavior that is similar to that observed in (1 0 0) silicon MOSFETs [15]. This reveals that at the lowest electron densities, the spin splitting is close to the cyclotron splitting, i.e., the product gm is strongly enhanced (by a factor of about 3).

We would like to emphasize that unlike (1 0 0) silicon MOSFETs with mobilities in excess of $\approx 2 \times 10^4$ cm^2 V^{-1} s^{-1}, the metallic temperature dependence of the $B = 0$ resistance is not observed below $T = 1.3$ K in our samples.

A typical temperature dependence of the amplitude, A, of the weak-field (sinusoidal) SdH oscillations for the normalized resistance, R_{xx}/R_0 (where R_0 is the average resistance),

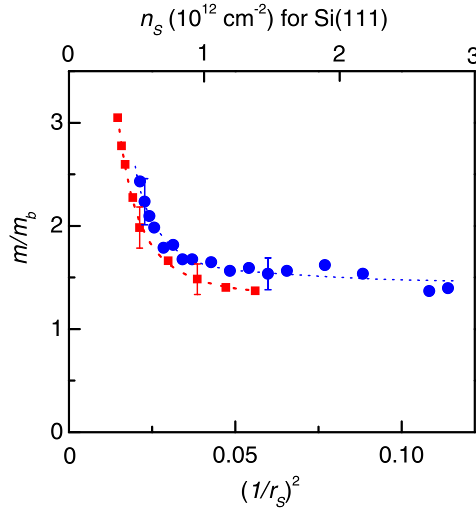

Figure 7. The effective mass (dots) in units of m_b as a function of $(1/r_s)^2 \propto n_s$. Also shown by squares are the data obtained in (1 0 0) Si MOSFETs [10]. The dashed lines are guides to the eye. (From [14].)

is displayed in figure 6. To determine the effective mass, we use the method of [16] extending it to low electron densities and temperatures. We fit the data for $A(T)$ using the formula

$$A(T) = A_0 \frac{2\pi^2 k_B T/\hbar\omega_c}{\sinh(2\pi^2 k_B T/\hbar\omega_c)},$$
$$A_0 = 4\exp(-2\pi^2 k_B T_D/\hbar\omega_c), \tag{2}$$

where $\omega_c = eB/mc$ is the cyclotron frequency, and T_D is the Dingle temperature [10, 17]. The latter is related to the level width through the expression $T_D = \hbar/2\pi k_B \tau$, where τ is the quantum scattering time [12]. In principle, temperature-dependent τ may influence damping of the SdH oscillations with temperature. In our experiment, however, possible corrections to the mass value caused by the temperature dependence of τ (and hence T_D) are within the experimental uncertainty which is estimated by data dispersion at about 10%. Note that the amplitude of the SdH oscillations follows the calculated curve down to the lowest achieved temperatures, which confirms that the electrons were in a good thermal contact with the bath and were not overheated. Applicability of equation (2) to strongly interacting 2D electron systems is justified by the coincidence of the enhanced mass values obtained in (1 0 0) silicon MOSFETs using a number of independent measurement methods including this one [9–11].

In figure 7, we show the so-determined effective mass in units of the cyclotron mass in bulk silicon, $m_b = 0.358m_e$ (where m_e is the free electron mass), as a function of $(1/r_s)^2 \propto n_s$. (For the two-valley case the ratio E_C/E_F that determines the system behavior is twice as large as the Wigner–Seitz radius r_s. Below, we will use the Wigner–Seitz radius with an average dielectric constant of 7.7 as the interaction parameter.) The effective mass sharply increases with decreasing electron density, its enhancement at low n_s being consistent with that of gm. The mass renormalization m/m_b versus the interaction parameter r_s is coincident within the experimental uncertainty with that found in (1 0 0) silicon MOSFETs where $m_b = 0.19m_e$ is approximately twice as small and the peak mobility is approximately one order of magnitude as large. Thus, we arrive at a conclusion that the relative mass enhancement is determined by

r_s, being independent of a 2D electron system. Note that the highest accessible r_s is different in different 2D electron systems.

We now discuss the results obtained for the effective mass. We stress that the strongly increased mass is observed in a dilute 2D electron system with relatively high disorder, as inferred from both the relatively low zero-field mobility and the absence of metallic temperature dependence of zero-field resistance. Moreover, the disorder does not at all influence the relative enhancement of the mass as a function of the interaction parameter. This allows us to claim that the mass enhancement is solely caused by electron–electron interactions. Our results also add confidence that the dilute system behavior in the regime of the strongly enhanced spin susceptibility $\chi \propto gm$—close to the onset of spontaneous spin polarization and Wigner crystallization—is governed by the effective mass.

The finding that in dilute 2D electron systems the effective mass is strongly enhanced remains basically unexplained, although there has been a good deal of theoretical work on the subject (see [2, 3, 18] and references therein). The latest theoretical developments include the following. Using a renormalization group analysis for multi-valley 2D systems, it has been found that the effective mass dramatically increases at disorder-dependent density for the metal–insulator transition while the g-factor remains nearly intact [19]. However, the prediction of disorder-dependent effective mass is not confirmed by our data. In the Fermi-liquid-based model of [20], a flattening at the Fermi energy in the spectrum that leads to a diverging effective mass has been predicted. Still, the expected dependence of the effective mass on temperature is not consistent with experimental findings.

Finally, we would like to note that moderate enhancements of the effective mass $m \approx 1.5m_b$ have been determined in 2D electron systems of AlAs quantum wells and GaAs/AlGaAs heterostructures because the lowest accessible densities are still too high [21, 22]. While the theories of, e.g., [23, 24] are capable of describing the experimental $m(n_s)$ dependence at $r_s \sim 1$, their validity at larger values of the interaction parameter is a problem.

4. Summary

We have found that in a dilute 2D electron system in (1 0 0) silicon, the Pauli spin susceptibility critically increases upon approaching a certain sample-independent electron density, behavior characteristic of a phase transition. This effect is not associated with the growth of the g-factor which remains practically constant and close to its 'non-interacting' value. Rather, it originates from dramatically increasing effective mass. A similar increase of the effective mass was also observed in (1 1 1) silicon. Remarkably, the mass renormalization, m/m_b, versus the interaction parameter r_s is in good agreement with that in (1 0 0) silicon MOSFETs. This gives evidence that the relative mass enhancement is system and disorder independent, and is solely determined by electron–electron interactions. The particular mechanism underlying the effective mass enhancement remains to be seen.

Acknowledgments

We gratefully acknowledge discussions with E Abrahams, A Gold, and A Punnoose. The work at Northeastern University was supported by the NSF grant DMR-0403026 and BSF grant #2006375. The work at ISSP was supported by the RFBR, RAS and the programme 'The State Support of Leading Scientific Schools'.

References

[1] Abrahams E, Kravchenko S V and Sarachik M P 2001 *Rev. Mod. Phys.* **73** 251

[2] Kravchenko S V and Sarachik M P 2004 *Rep. Prog. Phys.* **67** 1

[3] Shashkin A A 2005 *Phys.—Usp.* **48** 129

[4] Estibals O, Kvon Z D, Gusev G M, Arnaud G and Portal J C 2004 *Physica* E **22** 446

[5] Prus O, Yaish Y, Reznikov M, Sivan U and Pudalov V 2003 *Phys. Rev.* B **67** 205407

[6] Shashkin A A, Anissimova S, Sakr M R, Kravchenko S V, Dolgopolov V T and Klapwijk T M 2006 *Phys. Rev. Lett.* **96** 036403

[7] Shashkin A A, Kravchenko S V, Dolgopolov V T and Klapwijk T M 2001 *Phys. Rev. Lett.* **87** 086801

[8] Zala G, Narozhny B N and Aleiner I L 2001 *Phys. Rev.* B **64** 214204

[9] Shashkin A A, Kravchenko S V, Dolgopolov V T and Klapwijk T M 2002 *Phys. Rev.* B **66** 073303

[10] Shashkin A A, Rahimi M, Anissimova S, Kravchenko S V, Dolgopolov V T and Klapwijk T M 2003 *Phys. Rev. Lett.* **91** 046403

[11] Anissimova S, Venkatesan A, Shashkin A A, Sakr M R, Kravchenko S V and Klapwijk T M 2006 *Phys. Rev. Lett.* **96** 046409

[12] Ando T, Fowler A B and Stern F 1982 *Rev. Mod. Phys.* **54** 437

[13] Iwamoto N 1991 *Phys. Rev.* B **43** 2174
Kwon Y, Ceperley D M and Martin R M 1994 *Phys. Rev.* B **50** 1684
Chen G-H and Raikh M E 1999 *Phys. Rev.* B **60** 4826

[14] Shashkin A A, Kapustin A A, Deviatov E V, Dolgopolov V T and Kvon Z D 2007 *Phys. Rev.* B **76** 241302(R)

[15] Kravchenko S V, Shashkin A A, Bloore D A and Klapwijk T M 2000 *Solid State Commun.* **116** 495

[16] Smith J L and Stiles P J 1972 *Phys. Rev. Lett.* **29** 102

[17] Lifshitz I M and Kosevich A M 1955 *Zh. Eksp. Teor. Fiz.* **29** 730
Isihara A and Smrcka L 1986 *J. Phys. C: Solid State Phys.* **19** 6777

[18] Kravchenko S V, Shashkin A A, Anissimova S, Venkatesan A, Sakr M R, Dolgopolov V T and Klapwijk T M 2006 *Ann. Phys.* **321** 1588

[19] Punnoose A and Finkel'stein A M 2005 *Science* **310** 289

[20] Khodel V A, Clark J W and Zverev M V 2005 *Europhys. Lett.* **72** 256

[21] Vakili K, Shkolnikov Y P, Tutuc E, De Poortere E P and Shayegan M 2004 *Phys. Rev. Lett.* **92** 226401

[22] Tan Y W, Zhu J, Stormer H L, Pfeiffer L N, Baldwin K W and West K W 2005 *Phys. Rev. Lett.* **94** 016405

[23] Zhang Y and Das Sarma S 2005 *Phys. Rev.* B **72** 075308

[24] Asgari R and Tanatar B 2006 *Phys. Rev.* B **74** 075301